PRACTICAL SUPERCONDUCTOR DEVELOPMENT FOR ELECTRICAL POWER APPLICATIONS

ARGONNE NATIONAL LABORATORY

QUARTERLY REPORT FOR THE PERIOD ENDING MARCH 31, 2000

This is a multiyear experimental research program focused on improving relevant material properties of high-T_c superconductors (HTSs) and on development of fabrication methods that can be transferred to industry for production of commercial conductors. The development of teaming relationships through agreements with industrial partners is a key element of the Argonne (ANL) program.

Technical Highlights

Recent results are presented on $YBa_2Cu_3O_x$ (Y-123) coated conductors, silver-sheathed $(Bi,Pb)_2Sr_2Ca_2Cu_3O_x$ (Bi-2223) tapes, and applications development.

Pulsed Laser Deposition System

A pulsed laser deposition (PLD) system consisting of a 30.5-mm-diameter deposition chamber, 5.1-cm-diameter substrate holder (950°C maximum temperature capability), and Lambda Physik KrF excimer laser (248 nm) has been installed. Figure 1 shows the PLD system in operation. Resulting Y-123 films (≈1 μm thick) deposited on single-crystal substrates have exhibited critical current density (J_c) values of ≈2 MA/cm^2 (critical current I_c > 40 A) at 77 K, zero applied field, and $J_c \approx 7.2 \times 10^5$ A/cm^2 (I_c = 18 A) at 77 K in a field of 0.4 T. Y-123 films have also been deposited on ion-beam-assisted-deposition (IBAD) substrates; these samples are waiting for I_c measurements. Based on the measured biaxial textures of the substrates, these Y-123/IBAD samples are expected to exhibit J_c values at 77 K > 1 MA/cm^2.

Deposition of Buffer Layers on Coated Conductors

Biaxially textured thin films of MgO have been deposited by electron beam evaporation on moving Ni-alloy tapes as oriented buffer layers for coated conductors. The moving substrates were inclined with respect to the atomic vapor and translated through collimated dual-vapor sources. Growth anisotropy in the MgO and self-shadowing effects due to the inclined angle combine to create biaxial texture in the deposited thin films. MgO films grown to thicknesses of 2.0 μm with this inclined-substrate deposition (ISD) technique have yielded in-plane textures of 10–12° full-width half-maximum (FWHM). Results of a parametric study

DISCLAIMER

Fig. 1. Photograph of PLD system.

on the in-plane texture in short-length static-mode samples, along with preliminary results of long-length samples deposited under translating conditions, are summarized.

Next-generation wire technology based on HTSs requires a biaxially textured template layer onto which a superconductor will be coated. A major hurdle in bringing these wires to market has been the slow deposition rates and/or complex deposition geometries needed to deposit biaxially textured template layers.

We are investigating the processing dependence of texture development in MgO films deposited by ISD in order to optimize the deposition parameters required for continuous coating. ISD of MgO has proved effective in creating short-length biaxially textured Y-123 coated conductors (see, e.g., M. Bauer et al., IEEE Trans. Appl. Supercond. 9 (1999) 1502). We coated 0.5-m-long tapes by using a collimated-flux inclined substrate deposition (CF-ISD) geometry with feed rates of 6.1 cm/min. The texture in the MgO films was evaluated with four-circle X-ray diffraction and selected-area electron diffraction (SAED). Growth morphology and structure were investigated by transmission electron microscopy (TEM).

Hastelloy-C tapes were ultrasonically cleaned in acetone and methanol prior to loading in a reel-to-reel continuous deposition system. The system was designed to allow simultaneous deposition on two tapes. The feed mechanism and take-up reel

were designed to put the as-coated MgO tape in compression, with the strain < 5%. The tapes were inclined 40° with respect to the atomic vapor, which was created with a dual-electron-beam evaporation system. Evaporation was conducted in two zones; each contained a group of collimators that restricted the angular variance of the atomic flux to < 10°. The feed rate through the two collimated deposition zones was adjusted such that MgO was deposited to a thickness of 1.0 μm in a single pass. The deposition rate for continuous coating was 0.6 μm/min.

Cross-sectional TEM coupled with SAED allowed the investigation of texture development in ISD MgO as a function of thickness (Fig. 2). From intensity-versus-thickness plots of dark-field photomicrographs, we determined that the coalescence zone of MgO into textured films occurs at ≈900 nm. In-plane texture of the MgO on static samples exhibited little dependence on deposition rate (Fig. 3). Deposition on static samples also indicated that in-plane texture improved with an increase in sample inclination with respect to the vapor source; this in turn inclined the (200) face, which grows toward the vapor (Fig. 4).

The average in-plane FWHM of a 0.5-m-long tape deposited under continuous conditions, as measured with pole figures, was 24°. This value is the average FWHM measured from 10 positions along the tapes at approximately every 5 cm. The standard deviation of the FWHM was 1°, with the best value equal to 23°. These values are slightly higher than expected from the use of 10° collimators;

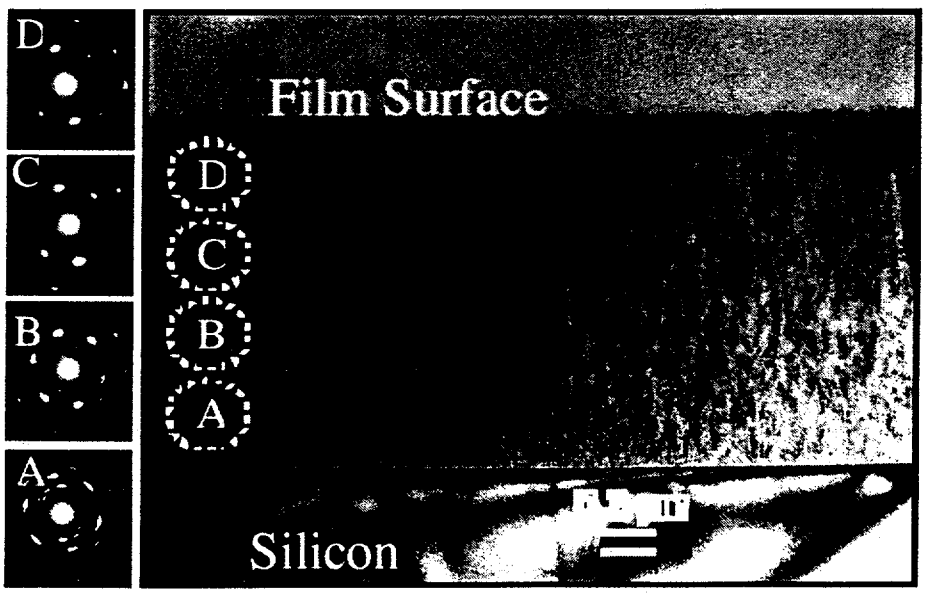

Fig. 2. TEM photomicrograph of statically processed film on Si, with SAED patterns at various film thicknesses.

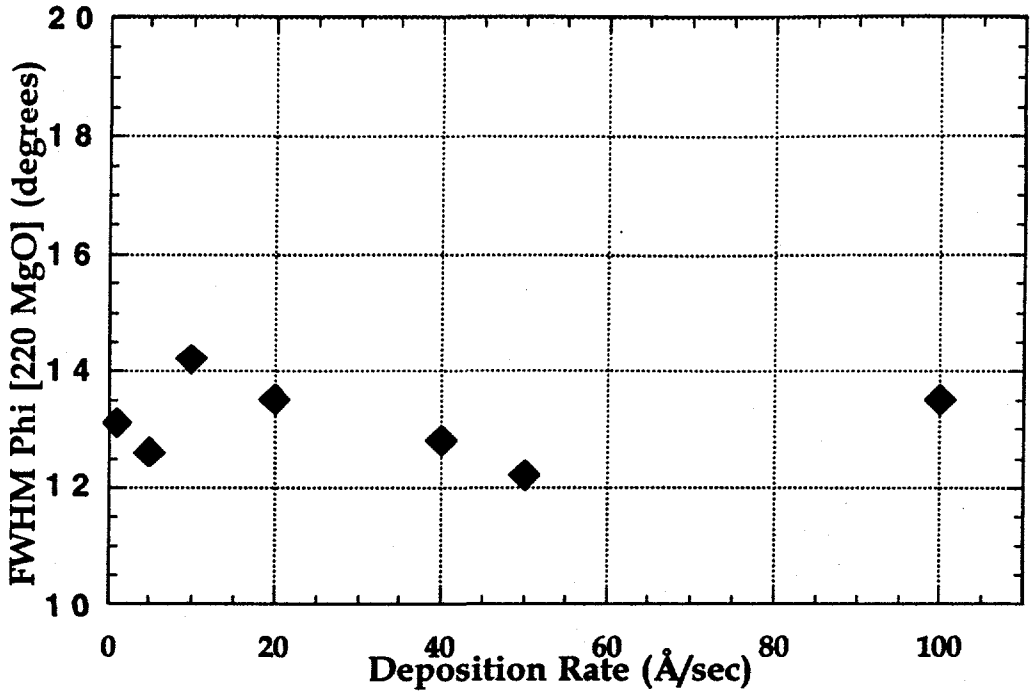

Fig. 3. In-plane texture of ISD MgO vs. deposition rate for 2.5-μm-thick films.

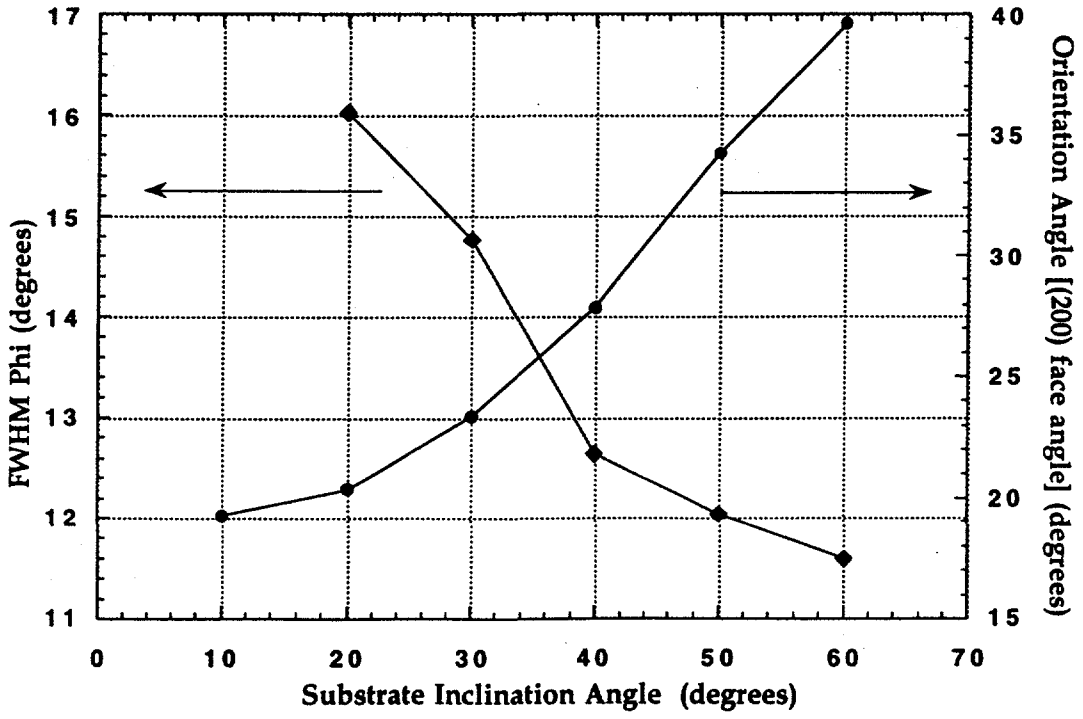

Fig. 4. In-plane FWHM and (200) face orientation of ISD MgO vs. substrate inclination angle in statically processed samples.

however, the measured FWHM are from films that are considerably thinner than the statically processed samples and the surface texture is expected to be much sharper than the bulk value. Work is in progress to address this issue by evaluating these layers with a thick homoepitaxial layer, to confirm the quality of the texture surface of the CF-ISD MgO films.

Bi-2223 Tape Development

Raman microspectroscopy and imaging techniques are being used to investigate key mechanistic features that influence the formation of layered Bi-based superconducting phases during the thermal treatment employed to produce Ag-sheathed Bi-2223 composite conductors. Recent information gained from these studies includes identification of the constituent phases in certain nonsuperconducting second phase (NSP) agglomerations that tend to resist dissipation as high-T_c phase formation proceeds to completion.

The experimental methods and instrumentation used in these measurements were reported previously (see, e.g., K. T. Wu et al., J. Mater. Res. 12 (1997) 1195). In brief, heat-treated Ag/Bi-2223 specimens were cast in epoxy and the casting was polished until the ceramic core of the specimen was exposed. Raman microscopy was used to examine the exposed polished cores, which were usually mounted in transverse view.

Figure 5 contains an example of the type of measurement that we typically make when using Raman microscopy techniques. The defocused Raman spectrum in Fig. 5 was obtained by spreading the excitation laser over the circled region indicated in the white-light image (WLI) of the specimen (in this case, a transversely mounted, fully processed, 19-filament Ag/Bi-2223 composite) and recording a dispersive (grating mode) Raman spectrum. The silver-sheath regions in the WLI shown in Fig. 5 have been darkened by image processing to provide contrast with the ceramic filaments. Portions of three ceramic filaments can be seen in the WLI.

From previous phase characterization studies, we know that the Raman features at 626, 570, and 520 cm^{-1} in defocused spectra are due to Bi-2223, $(Ca,Sr)_{14}Cu_{24}O_{41}$ (14/24 AEC), and $(Ca,Sr)_2CuO_3$ (2/1 AEC), respectively. Using the imaging Raman microscope in the filter mode, we determined the location within the circled area in the WLI from which the Raman scattering occurred at each of the three frequencies. These regions are shown by the three Raman images to the right of the WLI in Fig. 5. (Each of the three Raman images has been corrected to remove background (BG) effects.) In these three images, the white regions represent the locations of the phases scattering at the frequency indicated below each image.

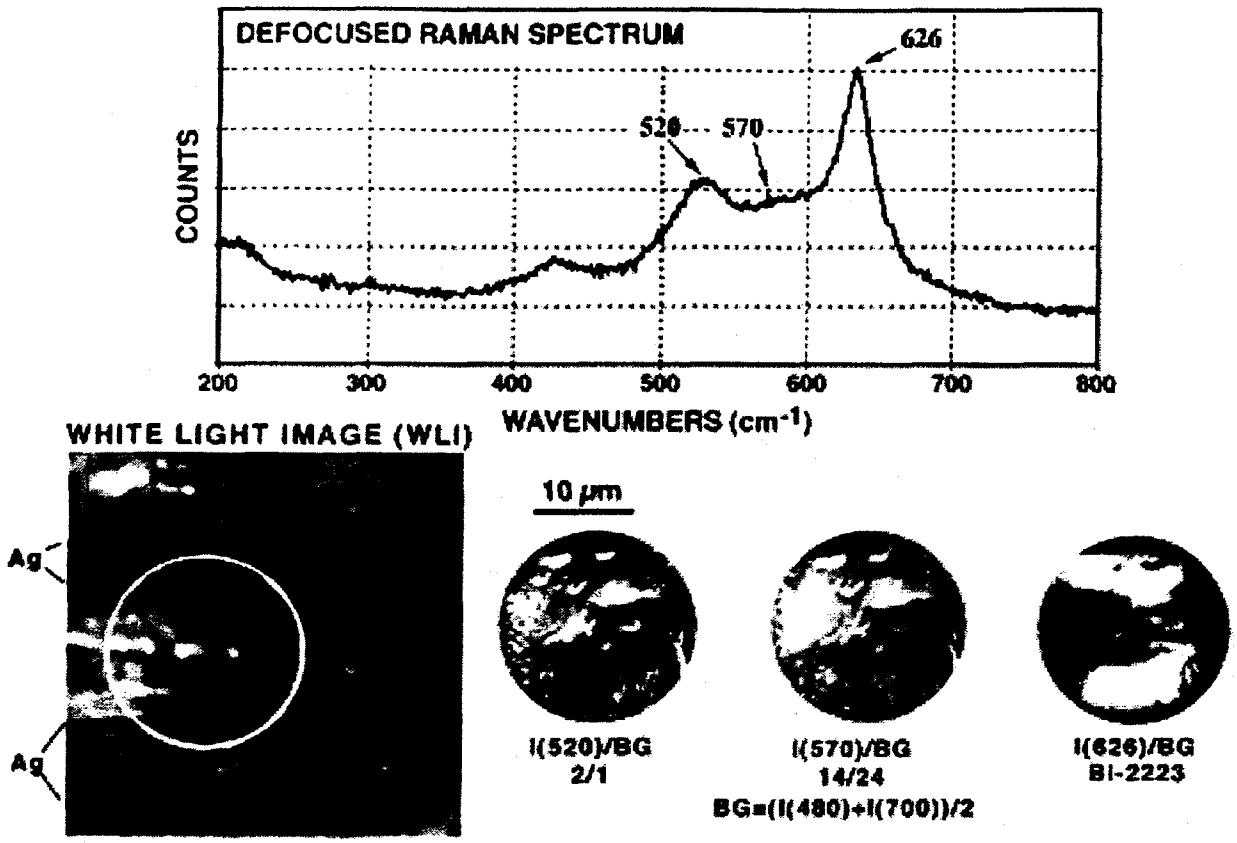

Fig. 5. Raman microscopy results for 19-filament Ag/Bi-2223 composite wire. White domains in Raman images I(520)/BG, I(570)/BG, and I(620)/BG indicate locations of the 2/1, 14/24, and Bi-2223, respectively, in white-light image.

The image of the 626 cm^{-1} feature, I(626)/BG, revealed that the layered Bi-2223 phase was located in bands along the Ag sheath. Images for the 570 and 520 cm^{-1} features revealed that the 14/24 and other nonsuperconducting phases tended to agglomerate and overlap in the midcore region of the filament. The appearance of overlapping phase domains was associated with the penetration depth of the excitation laser. NSP agglomeration appeared to be a key factor limiting the supercurrent capacity of the Ag/Bi-2223 composite conductor. Current Ag/Bi-2223 heat-treatment studies (in collaboration with American Superconductor Corp.) are focused on developing thermodynamics-based strategies for dissipating these agglomerates in multifilament wires.

Merged filaments constitute a second type of performance-limiting microstructural defect in multifilament Ag/Bi-2223 composite wires. Typically, when two filaments merge (Fig. 6), the resulting domain is characterized by poorly

developed Bi-2223 grain colonies and large agglomerations of NSPs. The defocused Raman spectrum in Fig. 6, obtained from the shaded region in the white-light image, shows evidence of 2/1 (its principal Raman band being indicated as image **a** in the defocused spectrum) and Bi-2223 (its principal Raman band being indicated as image **b** in the defocused spectrum). The white domains in the Raman images of images **a** and **b**, shown in Fig. 5, indicate the dominant locations of 2/1 and Bi-2223, respectively.

To obtain a clearer picture of the relative presence or absence of overlapping phases in Raman images of agglomerated regions, we have developed an image-processing procedure based on gray-scale inversion and subtraction. Inverting the gray scales for images **a** and **b** and then subtracting $\mathbf{a}^{-1}$ from $\mathbf{b}^{-1}$ produces an image in which white regions should highlight the general location of Bi-2223 and black regions should highlight the general location of 2/1. The result of this procedure is shown in Fig. 6. The whitest regions in the $(\mathbf{a}^{-1}-\mathbf{b}^{-1})$ image were where Bi-2223 was the more prominent phase; the darkest regions occurred where 2/1 was more prominent. Scanning electron microscopy/energy-dispersive spectroscopy (SEM/EDS) analyses of the regions shown in Fig. 6 yielded metallic element compositions that were in good agreement with the implications of the Raman imaging results. The type of phase congestion observed in the merge region under study in Fig. 2 was typical of almost all the merge zones we have examined in the course of this investigation.

Dissipation of Second Phases in Ag/Bi-2223 Composite Conductors

The discussion in the previous section of this report makes clear the need to greatly reduce or eliminate large, congested NSPs in multifilament Ag/Bi-2223 composite conductors. Over the past year, we have been investigating a heat-treatment protocol that either eliminates the NSPs or reduces them to the smallest possible size (preferably sub-micrometer). Based on the work of Holesinger et al. (presented at 1999 Annual Peer review) regarding the rubblizing effect that large NSPs have on Bi-2223 grain colonies during intermediate deformation, it seems particularly advantageous for this diminishment of the NSPs to take place during the first heat treatment (HT1), i.e., prior to intermediate deformation.

In the course of extensive studies of how temperature and oxygen partial pressure (pO_2) influence microstructural development during the heat treatment of Ag/Bi-2223 composites, we made the observation that for a given pO_2 in the range in which the Bi-2223 phase has appreciable stability (nominally 0.04 to 0.21 atm), there is an onset temperature for the growth of robust Bi-2223 grain colonies (a desirable effect) and another onset temperature for the persistent formation of large NSPs (an undesirable effect). This effect is illustrated in Fig. 7, wherein we refer to

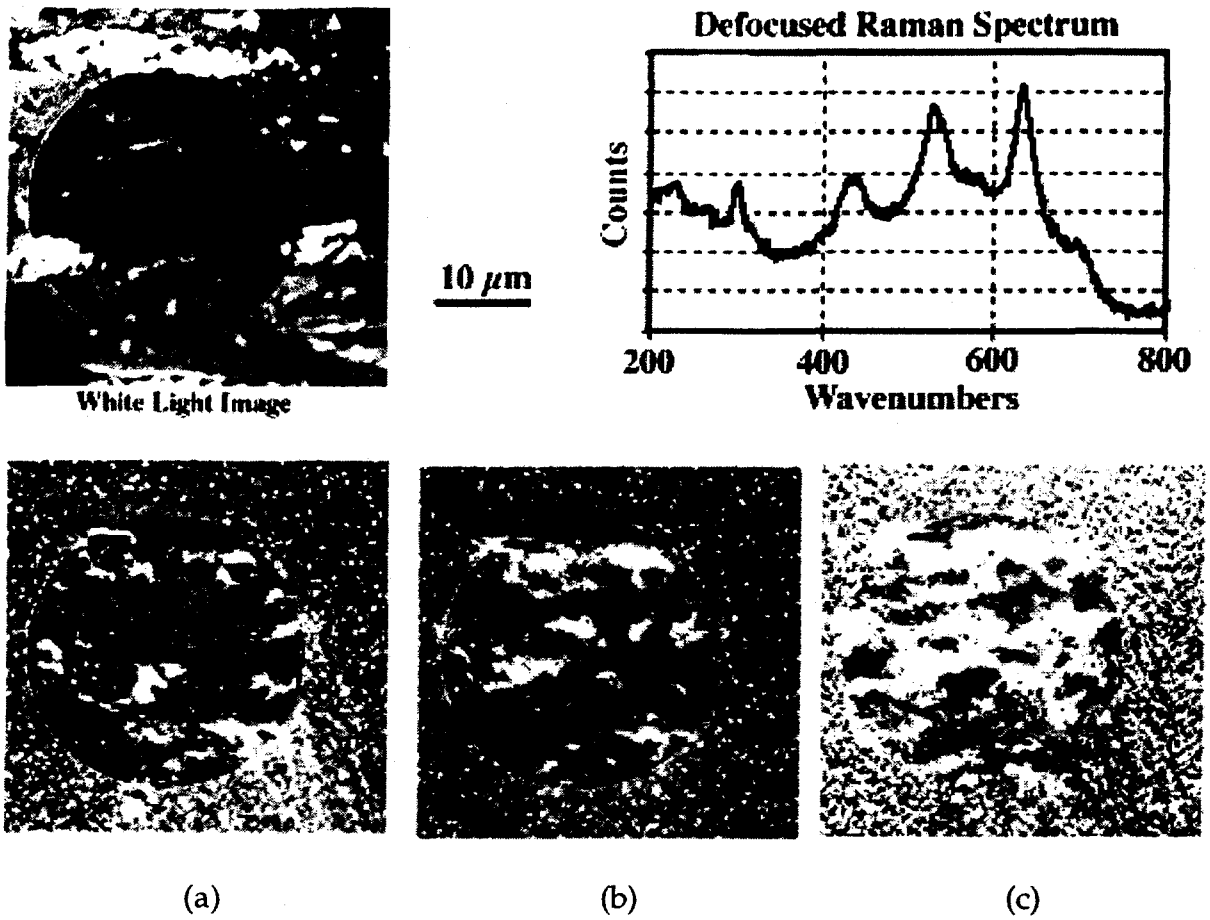

Fig. 6. Raman microscopy analysis of large merge zone between two filaments in 19-filament Ag/Bi-2223 composite wire. Images **a** and **b** in defocused Raman spectrum (circled region) are due to the 2/1 and Bi-2223, respectively. White areas in Raman images for (a) image **a** and (b) image **b** show dominant locations of 2/1 and Bi-2223 phases, respectively; (c) inverted/subtracted image ($\mathbf{a}^{-1}$–$\mathbf{b}^{-1}$) provides a map of general location of 2/1 (darkest regions) and Bi-2223 (lightest regions).

these two temperatures as the grain-growth takeoff temperature (GGTT) and the second-phase takeoff temperature (SPTT), respectively. Ideally, we want the GGTT to be well below the SPTT, but this is not generally the case. At the lowest pO_2 (0.04 atm), the SPTT is lower than the GGTT, and at 0.075 atm O_2, SPTT ≅ GGTT. However, at the higher pO_2s, the SPTT is slightly higher than the GGTT. From a processing point of view, we want to be on the SPTT curve, provided it lies at a temperature lower than the GGTT curve.

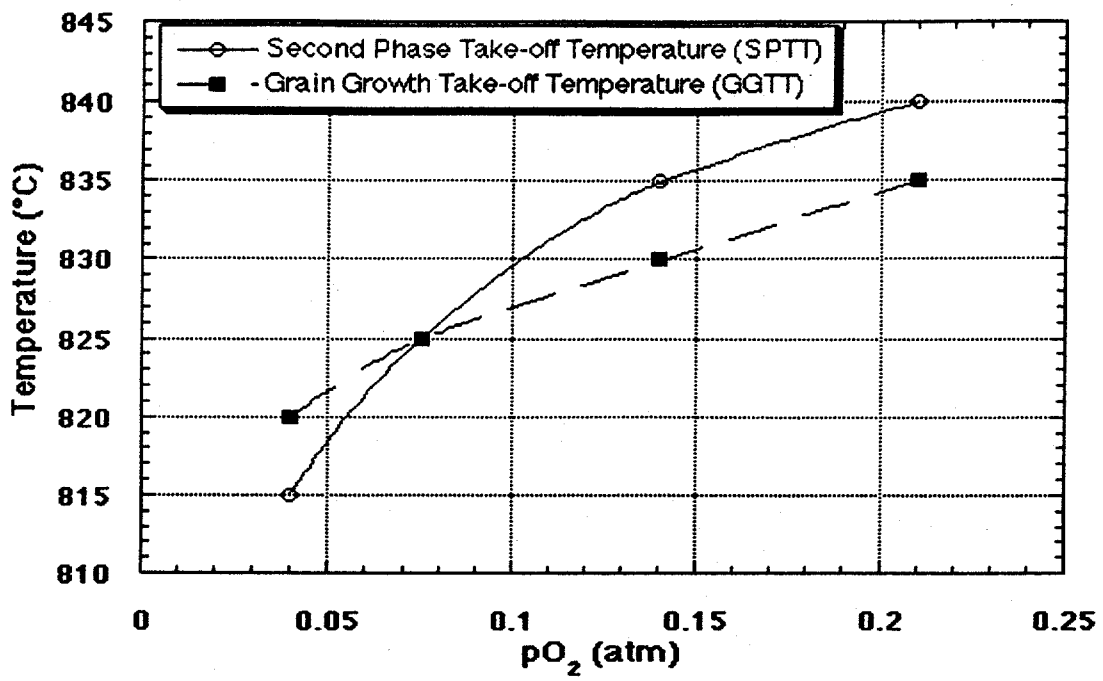

Fig. 7. Second-phase and grain-growth take-off temperatures for Ag/Bi-2223 composites as a function of pO_2.

The other important observation that we have made in the course of this work is that the composition of the NSPs varies significantly with pO_2 and temperature, from a CuO-dominated mix at low pO_2, to a $(Ca,Sr)_2CuO_3$-dominated mix at intermediate pO_2, to a $(Ca,Sr)_{14}Cu_{24}O_{41}$-dominated mix at the highest pO_2. This observation implies that it is possible to manipulate the constituent species of the NSP mix within the range of pO_2s in which the Bi-2223 phase has appreciable stability. One could do this by sliding along the GGTT curve between 0.075 and 0.21 atm O_2 and/or along the SPTT curve between 0.04 and 0.075 atm O_2. Accordingly, we have carried out HT1s on multifilament-type Ag/Bi-2223 composite specimens using several different combinations of pO_2 and temperature on the GGTT/SPTT lower bound in Fig. 7. A typical sliding heat treatment of this type (hereinafter call thermal slide heat treatment or TSHT) generally consists of the following sequence of steps:

1. ramping the temperature up to 825°C at 10°C/min in 0.075 atm O_2, and holding at 825°C for several hundred to 1000 min;

2. raising the temperature and pO_2 to 835°C and 0.21 atm O_2, respectively, and holding at those conditions for several hundred to 1000 min;

3. shifting the temperature and pO_2 to another point on the GGTT/SPTT lower bound (e.g., 815°C and 0.04 atm O_2) and holding for several hundred to 1000 min;

4. repeating combinations of the above heat treatments, then terminating the TSHT process by furnace-cooling the sample.

The TSHT methodology includes the condition that the variations must be made without ever crossing the lower (in terms of temperature) of the GGTT curve or the SPTT curve. This is done (depending on the direction one is moving along the GGTT/SPTT lower bound) by either lowering temperature first and then lowering pO_2, or pO_2 first then raising temperature. Termination of the treatment with a furnace cool (versus a rapid quench) is more appropriate for Ag/Bi-2223 wire manufacturing applications, because a rapid quench induces crack-causing stresses in the wire sample.

Development work on the TSHT process is being done in collaboration with American Superconductor (ASC) as part of the ASC-led Wire Development Group effort. The types of microstructures achieved in some of the better TSHT processing sequences we studied are shown in Figs. 8 and 9, which contain SEM images of transverse sections of 19-filament Ag/Bi-2223 composites after the TSHT procedure. Only a few second phases larger than 1 μm are noticeable in most of the 19 filaments in Fig. 8. The phase purity and sparse NSP content exhibited in Fig. 8 are considerably better than the norm for Ag/Bi-2223 composites. Figure 9 shows a high-magnification SEM image of another "better case" TSTH specimen. The sequence currently in use to produce "better case" HT1 specimens consists of 300 min at 825°C/0.075 atm O_2, then 1000 min at 835°C/0.21 atm O_2, then 1500 min at 825°C/0.075 atm O_2. X-ray diffraction examination of this HT1-type specimen indicated that the Bi-2223 to Bi-2212 ratio was ≈6.

Figure 10 presents the results of a computer-assisted SEM image analysis carried out for the sample that produced the image in Fig. 9. Inset a shows a grayscale histogram for a representative region of ceramic phase in the composite after manually erasing the silver by use of a standard image processing package. We know from previous studies that the 1–86 grayscale range corresponds to Bi-2223/Bi-2212, the 87–114 range corresponds to narrow transition regions between Bi-2223/Bi-2212 and the two AEC NSPs (2/1 and 14/24), the 115–156 range corresponds mainly to 14/24 AEC, and the 157+ range corresponds mainly to 2/1 AEC. Inset b shows the area fraction of each of the four ranges, and indicates that the total Bi-2223/Bi-2212 fraction is ≈90%.

In addition to achieving a lower area fraction of NSPs relative to conventional HT1 results, we also achieved microstructures with considerably fewer large NSPs. In collaboration with ASC, we have shown that some of our more effective TSHT treatments, when substituted for ASC's standard first heat treatment, lead to conductors with performance levels at least as good as ASC's best production wires manufactured to date. It is our hope that a fully optimized TSHT treatment coupled

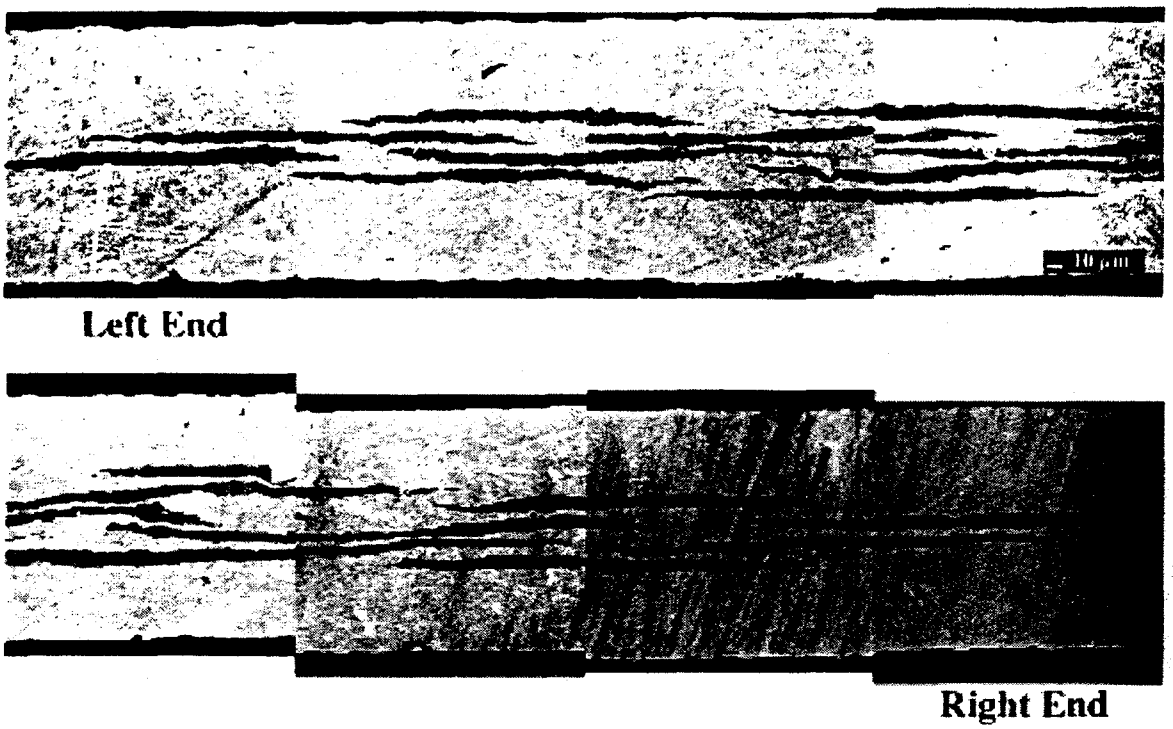

Fig. 8. Transverse section of a Bi-2223 composite specimen subjected to an optimized thermal-slide heat treatment.

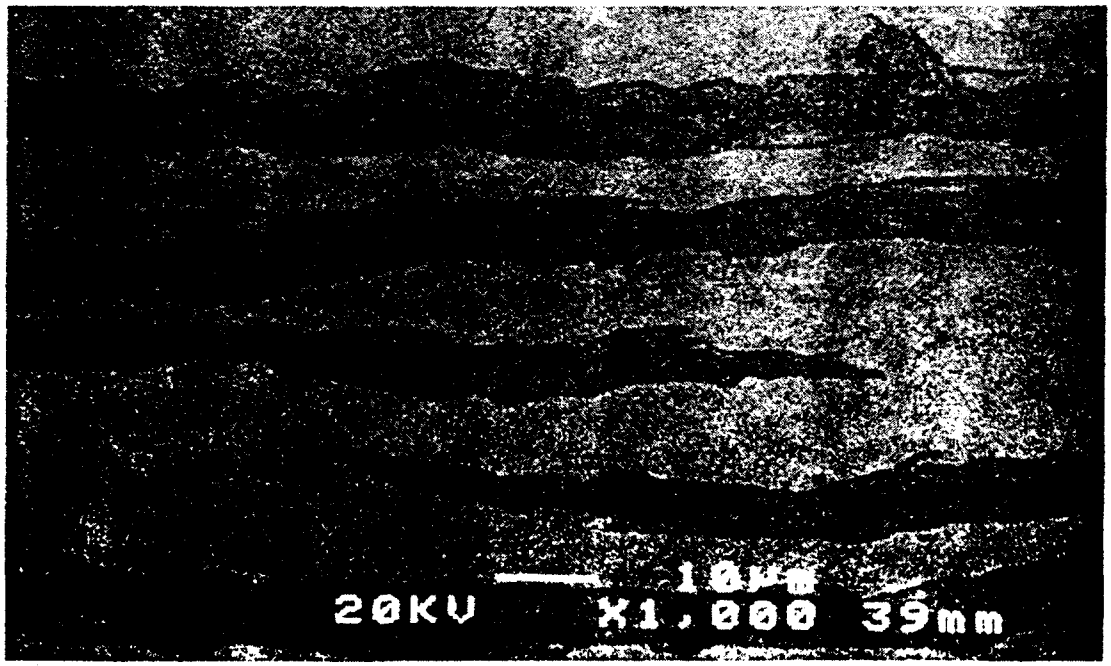

Fig. 9. High-magnification SEM image of representative segment of "better case" TSHT sample.

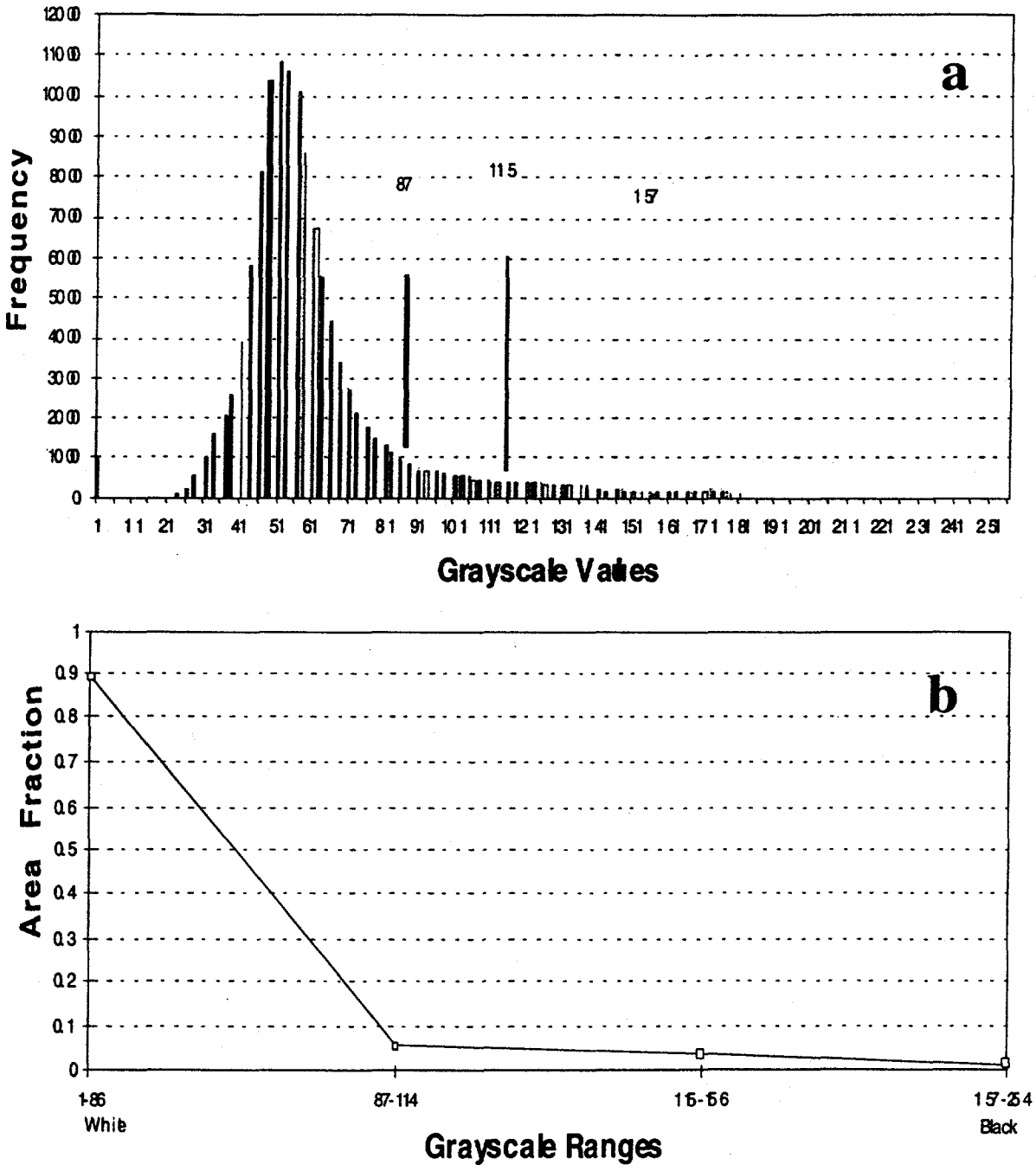

Fig. 10. (a) Grayscale values from SEM image in Fig. 9 and (b) area fractions for the four gray-scale regions indicated in (a); the four ranges (from left to right) correspond, respectively, to regions dominated by Bi-2223, Bi-2223/NSP transition zones, 14/24 AEC, and 2/1 AEC.

with a mating finishing treatment (yet to be developed for TSHTs) will yield an Ag/Bi-2223 conductor with 50–100% better performance properties than ASC's current production wires.

Work in progress on the TSHT process is aimed at determining (1) the optimum amount of time to spend at each temperature/pO_2 set point, (2) the most effective sequence of said set points, (3) the required number of visits to each set point, and (4) the optimum allowable Bi-2223 phase percentage at the end of a TSHT-type HT1. The last of these issues influences the final heat treatment that is carried out to heal the microstructural damage caused by the intermediate deformation done after HT1.

Current Sensor Development

In recent years, magneto-optical sensors have exhibited promise for use in high-power electronics applications. These sensors were first developed here to examine current paths in HTS conductors. They offer unique advantages over traditional sensors, such as shunt resistors, current transducers, Hall effect sensors, and magneto-resistive devices. These advantages include galvanic isolation, immunity to stray EMFs, absence of insertion losses, operation at elevated temperatures, and a frequency-independent response from DC to hundreds of MHz. The operating basis of magneto-optical sensors is the Faraday rotation of linearly polarized light occurring in the sensor material due to the magnetic field generated by the current to be measured. By incorporating the sensor material into a polarization-analyzing optical system (Fig. 11), a change in polarization is transformed into a change of the transmitted light intensity, which, in turn, is the measure of the current. Most present designs of optical high-current sensors, however, require that bulk magneto-optical components or long lengths of optical fiber encircle the current-carrying conductor.

We are developing a miniature high-current sensor that incorporates a new, epitaxial, rare-earth-substituted, iron-garnet, thin-film sensor material into a fiber-optical system. This design is made possible by the exceptionally large Faraday rotation and the unique magnetic properties of the sensor material. In typical epitaxial garnet films, magnetic moments are oriented perpendicular to the film plane, which leads to formation of stripe domains. The magneto-optical signal is a measure of the relative size of up- and down-magnetized domains, which change under the influence of an external field. In contrast, the new material employed here displays in-plane magnetic anisotropy, and the magneto-optical signal results from rotation of the magnetic moments under the influence of the external field. This allows for a linear response over a fairly large field and current range without the occurrence of hysteresis. In addition, because there is no need to average over a

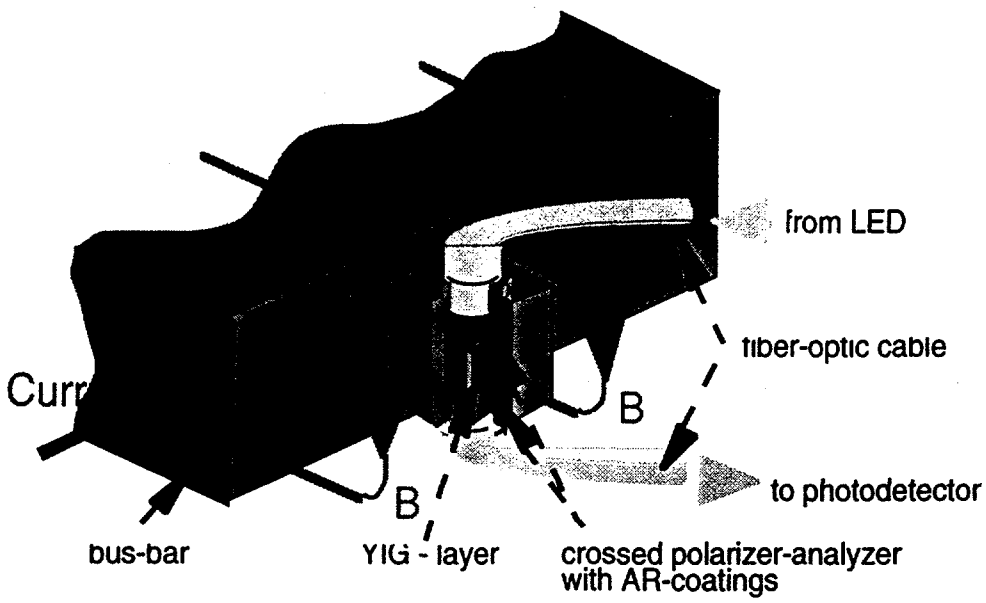

Fig. 11. Schematic diagram of current sensor mounted on bus bar. In transmission geometry, separate fibers are used for incoming and detected light.

sufficient number of domains, the miniaturization of the sensor to micrometer-scale is feasible, offering the possibility of direct integration of the sensor into high-power-electronics chips.

Future work would entail the construction of a prototype fiber-optical current sensor based on a new garnet magneto-optical material with improved characteristics. This work will include design and characterization of the sensor head and its integration into a fiber-optical readout system. We also propose to tailor the specifications of the sensor material (such as sensitivity, field of saturation, spectrum) to the desired application by changing the doping levels and growth conditions of the garnet films. Two proposals based on this work have been submitted to DOE.

Interactions

Balu Balachandran discussed the status of HTS program with Jim Daley on January 5 in Washington, DC.

Balu Balachandran visited Intermagnetics General Corp. to discuss the collaborative program on February 2.

Balu Balachandran attended the DOE wire workshop in St. Petersburg, FL, on February 10–11, 2000.

On February 18, Balu Balachandran attended the HTS cable dedication ceremony at Southwire Co in Carrollton, GA.

Mike Chudzik, Nicole Murphy, Victor Maroni, and Balu Balachandran presented papers at the M^2S-HTS conference, Houston, TX, Feb. 21–23.

Dr. Jeff Wolfenstine of the U.S. Army Laboratory in Adelphi, MD, visited on February 28 and 29. He presented a seminar on kinetic measurements in perovskite ceramics and met with several members of the program.

On March 1–3, Dr. Agusti Sin-Xicola of CNRS–Grenoble, France, visited and presented a seminar on synthesis of superconductor powders. Among topics discussed was preparation of nanoscale complex oxides.

On March 13–14, Balu Balachandran attended the TMS annual meeting in Nashville, TN, and presented a talk.

Prof. M. J. McNallan met with Balu Balachandran and Ken Goretta on March 24 to discuss methods for optimizing properties of Bi-2223 tapes that are sheathed in precipitation-hardened Ag alloys.

List of Publications

Published or presented

S. P. Athur (Texas Center for Superconductivity); U. Balachandran and K. Salama (Texas Center for Superconductivity), Melt Processing of YB-123 Tapes, paper presented at 6th Intl. Conf. on Materials and Mechanisms of Superconductivity and High-Temperature Superconductors, Houston, Feb. 20-25, 2000.

U. Balachandran, Coated Conductor Architecture: Inclined Substrate Deposition (ISD) of Textured Layer, oral presentation at DOE Wire Workshop, St. Petersburg, FL, Feb. 10-11, 2000.

U. Balachandran, HTS Power Technologies: Nanometers and Megawatts, oral presentation at 6th Intl. Conf. on Materials and Mechanisms of Superconductivity and High Temperature Superconductors, Houston, TX, Feb. 20-25, 2000.

U. Balachandran, T. R. Askew, Y. S. Cha, S. E. Dorris, J. T. Dusek, J. E. Emerson, B. L. Fisher, K. C. Goretta, K. E. Gray, J. R. Hull, M. T. Lanagan, M. Lelovic, V. A. Maroni, R. L. McDaniel, N. Merchant, D. J. Miller, J.-H. Park, J. J. Picciolo, and J. P. Singh, Practical Superconductor Development for Electrical Power Applications - Annual Report for FY 1999, ANL-99/20 (Dec. 1999).

U. Balachandran, M. P. Chudzik, R. A. Erck; C. R. Kannewurf (Northwestern U.); V. Selvamanickam and P. Haldar (IGC), IBAD/MOCVD-Based YBCO-Coated Conductor Development, Invited abstract presented at 2000 TMS Ann. Mtg., Nashville, TN, March 12-16, 2000.

M. P. Chudzik, R. A. Erck, U. Balachandran, Z. P. Luo, D. J. Miller; and C. R. Kannewurf (Northwestern U.), High-Rate Reel-to-Reel Continuous Coating of Biaxially Textured Magnesium Oxide Thin Films for Coated Conductors, Paper presented at 6th Intl. Conf. on Materials and Mechanisms of Superconductivity and High-Temperature Superconductors, Houston, Feb. 20-25, 2000.

J. R. Hull, Superconducting Bearings, Supercond. Sci. Technol. 13 (2000) R1-R15.

N. M. Murphy, S. E. Dorris, D. J. Miller, Z. P. Luo, H. Claus, and V. A. Maroni, Phase Formation and Superconductivity in PIT-Type (Bi,Pb)-1212, Paper presented at 6th Intl. Conf. on Materials and Mechanisms of Superconductivity and High-Temperature Superconductors, Houston, Feb. 20-25, 2000.

V. Selvamanickam, G. Galinski, C. Trautwein, G. Carota, J. DeFrank, P. Haldar (IGC); U. Balachandran, M. Chudzik: Y. Coulter, P. Arendt, B. Newnam, and D. E. Peterson (LASL), YBCO-Coated Conductor Development at IGC, Invited abstract presented at 6th Intl. Conf. on Materials and Mechanisms of Superconductivity and High-Temperature Superconductors, Houston, Feb. 20-25, 2000.

A. N. Terentiev (U. of Kentucky), J. R. Hull, and L. E. DeLong (U. of Kentucky), Depinning of Flux Lines and AC Losses in Magnet-Superconductor Levitation System, Abstract presented at 6th Intl. Conf. on Materials and Mechanisms of Superconductivity and High-Temperature Superconductors, Houston, Feb. 20-25, 2000.

Submitted

M. P. Chudzik, R. A. Erck, U. Balachandran; and C. R. Kannewurf (Northwestern U.), Ion Beam Energy and Divergence Dependence of Biaxial Texture in Cubic-Stabilized Zirconia Thin Films Grown by Ion-Beam-Assisted Deposition, Abstract to be presented at Applied Superconductivity Conf., Virginia Beach, VA, Sept. 17-22, 2000.

M. P. Chudzik, R. E. Koritala, U. Balachandran, Z. P. Luo, D. J. Miller; and C. R. Kannewurf (Northwestern U.), Mechanism and Processing Dependence of Biaxial Texture Development in Magnesium Oxide Thin Films Grown by Inclined-Substrate Deposition, Abstract to be submitted to Applied Superconductivity Conf., Virginia Beach, VA, Sept. 17-22, 2000.

Q. Y. Hu, M. Lelovic, U. Balachandran; V. Selvamanickam, P. Haldar (IGC); and L. M. Motowidlo (IGC Advanced Superconductors, Inc.), Fabrication of Ag-Sheathed $Bi_2Sr_2CaCu_2O_x$ Multifilamentary Wires for AC Applications, Abstract to be presented at 102nd Ann. Mtg. of American Ceramic Society, St. Louis, April 30-May 3, 2000.

R. E. Koritala, M. P. Chudzik, U. Balachandran, Z. P. Luo, D. J. Miller; and C. R. Kannewurf (Northwestern U.), TEM Investigation of Texture Development of Magnesium Oxide Buffer Layers, Abstract to be presented at Applied Superconductivity Conf., Virginia Beach, VA, Sept. 17-22, 2000.

M. Lelovic, U. Balachandran; V. Selvamanickam, and P. Haldar (IGC), Mechanical and Transport Current Properties of Laminated Ag-Sheathed Bi-2223 Tapes, Manuscript submitted to Superconductor Science and Technology (Dec. 1999).

B. C. Prorok, J.-H. Park, K. C. Goretta, U. Balachandran; and M. J. McNallan (U. of Illinois at Chicago), Strengthening of Ag/Bi-2223 Composite Wires by Internal Oxidation of Ag Alloys, Abstract to be presented at the 102nd Ann. Mtg. of American Ceramic Society, St. Louis, April 30-May 3, 2000.

B. C. Prorok, J.-H. Park, K. C. Goretta, U. Balachandran; and M. J. McNallan (U. of Illinois at Chicago), Internally Oxidized Ag/1.2 at.% Mg Sheaths for Bi-2223 Tapes, Abstract to be presented at Applied Superconductivity Conf., Virginia Beach, VA, Sept. 17-22, 2000.

V. Selvamanickam, G. Galinksi, G. Carota, J. DeFrank, C. Trautwein, P. Haldar (IGC); U. Balachandran, M. Chudzik; J. Y. Coulter, P. N. Arendt, S. R. Foltyn, B. Newman, and D. E. Peterson (LANL), High-Current Y-Ba-Cu-O Conductor by Metal Organic Chemical Vapor Deposition on Metal Substrates, Submitted to Physica C (Jan. 2000).

T. G. Truchan, M. P. Chudzik, R. A. Erck, K. C. Goretta, and U. Balachandran, Ion-to-Atom Arrival Ratio Dependence of In-Plane Texture in Yttria-Stabilized Zirconia Thin Films, Abstract to be presented at 102nd Ann. Mtg. of American Ceramic Society, St. Louis, April 30-May 3, 2000.

T. G. Truchan, M. P. Chudzik, B. L. Fisher, R. A. Erck, K. C. Goretta, and U. Balachandran, Effects of Ion-Beam Parameters on in-Plane Texture of Yttria-Stabilized Zirconia Thin Films, Abstract to be presented at Applied Superconductivity Conf., Virginia Beach, VA, Sept. 17-22, 2000.

1998–2000 Patents

Engineered flux pinning centers in BSCCO, TBCCO and YBCO superconductors
Kenneth C. Goretta, Michael T. Lanagan, Jieguang Hu, Dean J. Miller, Suvankar Sengupta, John C. Parker, U. Balachandran, Donglu Shi, and Richard W Siegel
U. S. Patent 5,929,001 (July 27, 1999).

Method and etchant to join Ag-clad BSCCO superconducting tape
Uthamalingam Balachandran, A. N. Iyer, and J. Y. Huang
U.S. Patent 5,882,536 (March 16, 1999).

Elongated Bi-based superconductors made by freeze dried conducting powders
Uthamalingam Balachandran, Milan Lelovic, and Nicholas G. Eror
U.S. Patent 5,874,384 (Feb. 23, 1999).

Thin film seeds for melt processing textured superconductors for practical applications
Boyd W. Veal, Arvydas Paulikas, Uthamalingam Balachandran, and Wei Zhong
U.S. Patent 5,869,431 (Feb. 9, 1999).

Superconductor composite
Stephen E. Dorris, Dominick A. Burlone, and Carol W. Morgan
U.S. Patent 5,866,515 (Feb. 2, 1999).

Surface texturing of superconductors by controlled oxygen pressure
Nan Chen, Kenneth C. Goretta, and Stephen E. Dorris
U.S. Patent 5,856,277 (Jan. 5, 1999).

Method for synthesizing and sinter–forging Bi–Sr–Ca–Cu–O superconducting bars
Nan Chen, Kenneth C. Goretta, and Michael T. Lanagan
U.S. Patent 5,821,201 (Oct. 13, 1998).

Mixed-mu superconducting bearings
John R. Hull and Thomas M. Mulcahy
U.S. Patent 5,722,303 (March 3, 1998).